References

ABRAMOWITZ, M. & STEGUN, I. (1972). *Handbook of Mathematical Functions*. New York: Dover.
BERTAUT, E. F. (1955). *Acta Cryst.* **8**, 823–832.
Computers in the New Laboratory – A Nature Survey (1981). *Nature*, **290**, 193–200.
CRAMÉR, H. (1951). *Mathematical Methods of Statistics*, section 12.6. Princeton Univ. Press.
FOSTER, F. & HARGREAVES, A. (1963). *Acta Cryst.* **16**, 1124–1133.
GRADSHTEYN, I. S. & RYZHIK, I. M. (1980). *Table of Integrals, Series and Products*, entry: 6.682(4). New York: Academic Press.
HAUPTMAN, H. & KARLE, J. (1953). *Acta Cryst.* **6**, 136–141.
HEARN, A. C. (1973). *REDUCE 2 User's Manual*. Univ. of Utah, Salt Lake City, Utah, USA.
KARLE, J. & HAUPTMAN, H. (1953). *Acta Cryst.* **6**, 131–135.
KLUG, A. (1958). *Acta Cryst.* **11**, 515–543.
LIPSON, H. & WOOLFSON, M. M. (1952). *Acta Cryst.* **5**, 680–682.
ROGERS, D. & WILSON, A. J. C. (1953). *Acta Cryst.* **6**, 439–449.
SHMUELI, U. (1979). *Acta Cryst.* A**35**, 282–286.
SHMUELI, U. (1982). *Acta Cryst.* A**38**, 362–371.
SHMUELI, U. & KALDOR, U. (1981). *Acta Cryst.* A**37**, 76–80.
SHMUELI, U. & WILSON, A. J. C. (1981). *Acta Cryst.* A**37**, 342–353.
SHMUELI, U. & WILSON, A. J. C. (1982). In *Crystallographic Statistics: Progress and Problems*, edited by S. RAMASESHAN, M. F. RICHARDSON & A. J. C. WILSON, pp. 83–97. Bangalore: Indian Academy of Science.
SRINIVASAN, R. & PARTHASARATHY, S. (1976). *Some Statistical Applications in X-ray Crystallography*. Oxford: Pergamon Press.
SZEGÖ, G. (1939). *Orthogonal Polynomials*, sections 2.1–2.5. New York: American Mathematial Society.
WATSON, G. N. (1922). *Theory of Bessel Functions*. Cambridge Univ. Press.
WILSON, A. J. C. (1942). *Nature (London)*, **150**, 151, 152.
WILSON, A. J. C. (1949). *Acta Cryst.* **2**, 318–321.
WILSON, A. J. C. (1952). *Research*, **5**, 589–590.
WILSON, A. J. C. (1956). *Acta Cryst.* **9**, 143–144.
WILSON, A. J. C. (1978). *Acta Cryst.* A**34**, 986–994.
WILSON, A. J. C. (1980*a*). *Acta Cryst.* A**36**, 945–946.
WILSON, A. J. C. (1980*b*). *Acta Cryst.* A**36**, 929–936.

Acta Cryst. (1983). A**39**, 233–245

Further Properties of a Gaussian Model of Disorder

BY T. R. WELBERRY AND C. E. CARROLL

Research School of Chemistry, Australian National University, PO Box 4, *Canberra, ACT* 2600, *Australia*

(*Received* 16 *August* 1982; *accepted* 7 *October* 1982)

Abstract

A generalization of a previously described Gaussian growth-disorder model is described. The properties of this general model are discussed in relation to the more restricted but more easily simulated growth-disorder model. Optical diffraction patterns of realizations obtained by Monte Carlo procedures are presented for two possible applications of the model. The extra degree of freedom provided by the generalization enables a greater diversity of diffraction patterns to be achieved. In particular, it is possible to produce realizations having an approximately isotropic correlation field. The relationship between the Gaussian model and the Hosemann paracrystal is discussed.

1. Introduction

In previous papers (Welberry, 1977; Welberry, Miller & Pickard, 1979; Welberry, Miller & Carroll, 1980; Welberry & Carroll, 1982), we have described a series of stochastic models of disorder called 'growth-disorder models', which enable the rapid production of optical diffraction masks representing disordered lattices. Such diffraction masks have been the principal tool in a number of studies of disorder phenomena reported recently, including orientational disorder in molecular crystals (Welberry, Jones & Epstein, 1982), cation framework distortions in materials with ferroelectric properties (Welberry, 1982), and highly disordered lattices known as paracrystals which are used in the study of polymers and amorphous materials (Welberry, Miller & Carroll, 1980).

The efficacy of the growth-disorder models for the purpose of optical diffraction mask making relies on the simple and rapid growth algorithm which enables suitably large realizations of disordered lattices containing predetermined short-range-order properties to be produced. The disordered distributions which may be produced by this means are, however, not the most general possible on a given lattice, and often approximations to the desired distribution must be made. Access to realizations of more general distributions can only be obtained *via* lengthy Monte Carlo iterative procedures and for routine usage such methods are not feasible. In this paper we explore some aspects of the relationship between a growth-disorder model and its

0567-7394/83/020233-13$01.50

more general counterpart, with a view to assessing the extent of the approximation made in using growth-disorder models to describe observed disorder phenomena.

Although our early interest was in binary models, since many disorder problems are naturally expressed in terms of binary variables, the most generally useful model developed to date is one which uses a multivariate Gaussian representation of lattice distributions. Versions of this model applicable to three (3D) or higher dimensions are just as readily used as the basic 2D model (Welberry & Carroll, 1982). Moreover, a method of converting Gaussian to binary variables was reported and this allows wide application of the model.

The 2D version of this Gaussian model, first described in the context of paracrystalline lattices (Welberry, Miller & Carroll, 1980), is formulated in terms of the probability of the four local variables X_A, X_B, X_C, X_D at the corners of the unit square (see Fig. 1). The most general probability density for these variables is $P(X_A, X_B, X_C, X_D)$, which may be factorized using conditional probabilities:

$$P(X_A,X_B,X_C,X_D) = P(X_A)\,P(X_B/X_A)\,P(X_C/X_A,X_B) \times P(X_D/X_A,X_B,X_C). \quad (1)$$

The special case of this which corresponds to a growth-disorder model occurs when

$$P(X_C/X_A,X_B) = P(X_C/X_A), \quad (2)$$

i.e. when X_C is conditionally independent of X_B given X_A. When this condition is satisfied realizations may be grown in the way described by Welberry & Carroll (1982). These general considerations are applicable whether X is a binary, Gaussian or any other type of random variable.

For $P(X_A, X_B, X_C, X_D)$ having rectangular (*pmm*) symmetry, the growth-disorder model has three degrees of freedom and distributions may be obtained for which the lattice averages

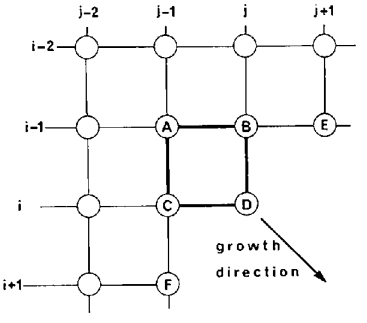

Fig. 1. Lattice-site labelling for the 2D Gaussian model. For the growth-disorder special case, realizations may be obtained in the manner indicated by adding points one at a time using equations (1) and (2).

$$\sigma^2 = \langle X_{i,j}^2 \rangle$$
$$r = \langle X_{i,j} X_{i+1,j} \rangle / \sigma^2 \quad (3)$$
$$s = \langle X_{i,j} X_{i,j+1} \rangle / \sigma^2$$

may be chosen independently. Here $\langle\ \rangle$ denotes the average over the population of Gaussian models. We can also evaluate it as the average over all values of i and j, using only one realization of the model. The averages in (3) represent a single-site distribution and two inter-site correlation coefficients between nearest-neighbouring points along the axial directions. It is a property of all such symmetric growth-disorder models that the diagonal correlation coefficient $t = \langle X_{i,j} X_{i+1,j+1} \rangle / \sigma^2$ is the product of the primary axial correlations r and s. This property stems directly from the conditional independence relation (2) and the removal of that condition allows t to vary independently. One of the main purposes of the present work is to explore the significance of variations of t for the diffraction properties of the model.

A second related feature of the growth-disorder-model formulation that is perhaps less than satisfactory is the asymptotic behaviour of the correlation coefficients at large distances. The form of the general correlation coefficient is given by

$$\rho_{m,n} = r^{|m|}\, s^{|n|} \quad (4)$$

so that it is apparent that correlations fall to zero more rapidly along diagonal directions than along the axes. Such a property is not the case, for example, for the Ising model near its critical temperature, where a much greater degree of isotropy occurs (Cheng & Wu, 1967).

In a previous paper we also described the relationship between a Gaussian growth-disorder model and the paracrystal model (see Hosemann & Bagchi, 1962) of highly distorted lattices used by workers in the area of polymers and amorphous materials. It is evident in that field that the lack of isotropy of the correlation field for the 'ideal paracrystal' is of concern (see Brämer & Ruland, 1976) and attempts to improve the isotropy by the introduction of the 'real paracrystal' do not appear to offer a solution to this problem. More recently Hosemann (*e.g.* Hosemann, Vogel, Weick & Baltá-Calleja, 1981) has made use of the so-called α^* law to overcome some of the problems of the paracrystal concept. This essentially turns the 'paracrystal' into an inhomogeneous model where 'grains' of distorted lattice are allowed to grow to a relatively small finite limit with the distortions increasing towards the boundaries. This may offer a more realistic solution to practical problems in this area where homogeneity is not necessarily a requirement. It is, however, still of interest to explore the properties of a homogeneous model, if only to justify the necessity to discard it for use in this context.

In the sections that follow we develop the theory of a general Gaussian model with emphasis on those aspects mentioned above, and illustrate these with sample realizations obtained by Monte Carlo methods. The number of sample realizations has of necessity been kept to a minimum because of the considerable computational effort required to obtain realizations of sufficient size to give reasonably noise-free optical diffraction patterns.

2. The general 2D Gaussian model on a square lattice

We discuss in this paper the general case of the Gaussian model which was formulated in a previous paper (Welberry & Carroll, 1982). The growth-disorder-model special case of this model was discussed in detail in that paper and some aspects pertaining to the paracrystal problem in an earlier paper (Welberry, Miller & Carroll, 1980). We refer the reader to these papers for details of the formulation but here recall that $X_{i,j}$ is a Gaussian-distributed random variable at the site i,j of a square lattice of N sites wrapped around a torus, and the multivariate probability density of these variables is given as

$$P = \frac{\exp\left[-\frac{1}{2}\sum_{\alpha\beta} X_\alpha (V^{-1})_{\alpha\beta} X_\beta\right]}{(2\pi)^{N/2}(\det V)^{1/2}}$$

$$= \left(\exp\left\{-\tfrac{1}{2}\sum_i\sum_j X_{i,j}[AX_{i,j} + 2BX_{i+1,j} + 2CX_{i,j+1} + 2D(X_{i+1,j-1} + X_{i+1,j+1})]\right\}\right) \times [(2\pi)^{N/2}(\det V)^{1/2}]^{-1}, \quad (5)$$

where V is the variance–covariance matrix. A must be positive in order to have a total probability that can be normalized to unity. This Gaussian probability density was treated briefly by Moran (1973*b*) in a paper that examined Markov processes on a square lattice. The particularly simple form of the inverse matrix V^{-1} given by (5) arises because of the assumptions of translational invariance of the statistical properties, of the (*pmm*) symmetry of the multi-variate distribution, and that only interactions between nearest neighbours along axial and diagonal directions are non-zero. The lattice averages σ^2, r, s, t were defined in § 1 in terms of elements of the variance–covariance matrix V. We show that specification of these four primary lattice averages allows the determination of the parameters A, B, C, D in the probability density (5), and *vice versa*. After computation of A, B, C, D, (5) may be used to obtain further properties of the model *via* Monte Carlo simulations or analytical calculations.

The formulae for σ^2, r, s, t in terms of A, B, C, D are obtained by inverting V^{-1}, an $N \times N$ matrix specified by (5). This inversion is greatly simplified by the translational invariance, which determines the form of the eigenvectors. The process of inversion is described by Moran (1973*a*). The eigenvalues of V^{-1} are $A + 2B\cos\lambda + 2C\cos\mu + 4D\cos\lambda\cos\mu$, where λ and μ are index variables that change only in discrete steps. The matrix elements of V are the variances and covariances $\langle X_{i,j} X_{i',j'}\rangle$, which depend only on $m = i - i'$ and $n = j - j'$, because of the translational invariance. This general matrix element is equal to

$$\langle X_{mn} X_{00}\rangle = \sigma^2 \rho_{m,n} = \frac{1}{N}\sum_\lambda\sum_\mu \exp(im\lambda + in\mu)(A + 2B\cos\lambda + 2C\cos\mu + 4D\cos\lambda\cos\mu)^{-1}, \quad (6)$$

where i is now the imaginary unit, and the sums run over all allowed values of λ and μ. When the number of rows and the number of columns in our lattice both tend to infinity, we obtain a double integral as the limit of (6).

As particular cases of this result, the primary lattice averages are given by

$$\sigma^2 = \int_{-\pi}^{\pi}\int \frac{d\lambda\, d\mu}{(2\pi)^2} \times (A + 2B\cos\lambda + 2C\cos\mu + 4D\cos\lambda\cos\mu)^{-1}, \quad (7)$$

$$\sigma^2 r = \int_{-\pi}^{\pi}\int \frac{d\lambda\, d\mu}{(2\pi)^2}\cos\lambda \times (A + 2B\cos\lambda + 2C\cos\mu + 4D\cos\lambda\cos\mu)^{-1}, \quad (8)$$

$$\sigma^2 s = \int_{-\pi}^{\pi}\int \frac{d\lambda\, d\mu}{(2\pi)^2}\cos\mu \times (A + 2B\cos\lambda + 2C\cos\mu + 4D\cos\lambda\cos\mu)^{-1}, \quad (9)$$

$$\sigma^2 t = \int_{-\pi}^{\pi}\int \frac{d\lambda\, d\mu}{(2\pi)^2}\cos\lambda\cos\mu \times (A + 2B\cos\lambda + 2C\cos\mu + 4D\cos\lambda\cos\mu)^{-1}. \quad (10)$$

These four equations provide the basis for computation of A, B, C, D as functions of σ^2, r, s, t.

Our multivariate Gaussian distribution exists only if the parameters r, s, t or A, B, C, D lie within certain bounds. We consider first the four-variable Gaussian distribution for variables associated with an elementary

unit square in the lattice. Their variance–covariance matrix is

$$\sigma^2\begin{pmatrix} 1 & r & s & t \\ r & 1 & t & s \\ s & t & 1 & r \\ t & s & r & 1 \end{pmatrix} \tag{11}$$

and we assume that σ^2 is positive. The four-variable Gaussian probability density can be normalized to unity only if this matrix has positive eigenvalues. This requires r, s, t to lie between -1 and $+1$, and the determinant of (11) to be positive. Since the determinant factors into linear functions, the conditions on r, s, t become

$$\begin{aligned} 1 + r + s + t &> 0 \\ 1 + r - s - t &> 0 \\ 1 - r + s - t &> 0 \\ 1 - r - s + t &> 0. \end{aligned} \tag{12}$$

The point having Cartesian coordinates (r,s,t) must lie inside a certain tetrahedron. Conditions that must be satisfied by A, B, C, D are derived similarly, from the requirement that (5) can be normalized to unity. We must have

$$A + 2B\cos\lambda + 2C\cos\mu + 4D\cos\lambda\cos\mu > 0 \tag{13}$$

for all allowed values of λ and μ. The distinction between allowed values and real values is negligible when the lattice is sufficiently large, and the conditions

$$\begin{aligned} A + 2B + 2C + 4D &> 0 \\ A + 2B - 2C - 4D &> 0 \\ A - 2B + 2C - 4D &> 0 \\ A - 2B - 2C + 4D &> 0 \end{aligned} \tag{14}$$

are found. The resulting requirement that A must be positive was mentioned above. The point having Cartesian coordinates $(2B/A,2C/A,4D/A)$ must lie inside the same tetrahedron as for (r,s,t).

If A, B, C, D satisfy (14), we can compute σ^2, r, s, t from (7)–(10). Conversely, if σ^2 is positive and (12) is satisfied, we can compute A, B, C, D; it can be shown that the solution for A, B, C, D exists and is unique. The computations leading from A, B, C, D to σ^2, r, s, t and *vice versa* are described in the Appendix. When A, B, C, D are known we can compute further properties of the model, as described in the following sections.

3. Correlation coefficients

The correlation coefficient $\langle X_{mn}X_{00}\rangle/\sigma^2 = \rho_{m,n}$ is given by (6) or the corresponding double integral. In this respect, our two-dimensional model is somewhat simpler than the Ising model, in which the number of definite integrals involved in the formula for a correlation coefficient increases with $|m|$ and $|n|$ (Montroll, Potts & Ward, 1963). The correlation coefficient for our model can be written as

$$\rho_{m,n} = \frac{1}{2\pi\sigma^2}\int_{-\pi}^{\pi} \exp(im\lambda)[\exp(i\mu_\lambda)]^{|n|} \times [(A + 2B\cos\lambda)^2 - 4(C + 2D\cos\lambda)^2]^{-1/2}\,d\lambda, \tag{15}$$

where

$$\exp(i\mu_\lambda) = \{-(A + 2B\cos\lambda) + [(A + 2B\cos\lambda)^2 - 4(C + 2D\cos\lambda)^2]^{1/2}\} \times [2(C + 2D\cos\lambda)]^{-1}.$$

If $m^2 + n^2$ is not very large, numerical integration of (15) is feasible, and we have used a Gaussian quadrature scheme to explore the correlation field. In the special case of $AD - BC = 0$, the denominator in (6) becomes

$$A[1 + (2B/A)\cos\lambda][1 + (2C/A)\cos\mu],$$

and the double integral is easily evaluated. We find

$$\langle X_{mn}X_{00}\rangle = \sigma^2 r^{|m|}s^{|n|} = \sigma^2\rho_{m,n}, \tag{16}$$

where r is a function of B/A and s is a function of C/A. Using these functions, we obtain

$$\begin{aligned} A &= \frac{(1 + r^2)(1 + s^2)}{\sigma^2(1 - r^2)(1 - s^2)} \\ B &= \frac{-r(1 + s^2)}{\sigma^2(1 - r^2)(1 - s^2)} \\ C &= \frac{-s(1 + r^2)}{\sigma^2(1 - r^2)(1 - s^2)} \\ D &= \frac{rs}{\sigma^2(1 - r^2)(1 - s^2)}. \end{aligned} \tag{17}$$

Note that (16) implies $t = rs$. Hence, $t \neq rs$ implies $AD - BC \neq 0$. It can be shown that $AD - BC$ and $t - rs$ always have opposite signs.

So far we have described the statistical properties of the Gaussian model without reference to particular diffraction applications. In the sections that follow we describe two such applications. The first was chosen primarily for its simplicity and the second because of its relevance to the 'paracrystal' problem.

4. Random form factors

We suppose that we have an atom at each site of a square lattice, and that the atomic form factors are

random variables having a multivariate Gaussian distribution. This model is a simple and concrete application of the Gaussian model described above. In this section, we consider this simple model, and obtain an explicit formula for the diffracted intensity.

Suppose that **l** is a vector, with integer components m and n, from the origin to a lattice site, and that f_l is the corresponding random form factor. The intensity of scattered waves is

$$|\sum_l f \exp[i(\mathbf{Q}.\mathbf{l})]|^2$$
$$= \sum_{mn} \sum_{m'n'} f_{mn} f_{m'n'} \exp[iQ_x(m-m') + iQ_y(n-n')],$$

where **Q** is the scattering vector with components Q_x and Q_y, and we assume f is real. Since our Gaussian model has translational symmetry, the average intensity is proportional to

$$I(\mathbf{Q}) = \sum_{m,n} \langle f_{mn} f_{00} \rangle \exp[i(Q_x m + Q_y n)].$$

The average appearing here can be written as

$$(\langle f \rangle)^2 + \langle (f_{mn} - \langle f \rangle)(f_{00} - \langle f \rangle) \rangle, \qquad (18)$$

because $\langle f_{mn} \rangle = \langle f \rangle$ is independent of m and n. The first term in (18) corresponds to Bragg diffraction, and we set the second term equal to $\langle X_{mn} X_{00} \rangle$, given by (6). The resulting intensity of diffuse scattering is

$$I(\mathbf{Q})_{\text{diff}} = \sum_{m,n} \frac{\exp[i(Q_x m + Q_y n)]}{N}$$
$$\times \sum_{\lambda} \sum_{\mu} \exp[i(m\lambda + n\mu)](A + 2B\cos\lambda + 2C\cos\mu + 4D\cos\lambda\cos\mu)^{-1}.$$

We need evaluate this quadruple sum only for very large lattices, for which the allowed values of λ and μ have arbitrarily small spacing. We assume that Q_x and Q_y are equal to allowed values of λ and μ respectively, which simplifies the sums over m and n. Then the sums over λ and μ are easily performed, and

$$I(\mathbf{Q})_{\text{diff}} = [A + 2B\cos(Q_x) + 2C\cos(Q_y) + 4D\cos(Q_x)\cos(Q_y)]^{-1}. \qquad (19)$$

This result is exact in the limit of an infinite lattice. The conditions (14) now appear as conditions that $I(\mathbf{Q})_{\text{diff}}$ is always positive. If $A + 2B + 2C + 4D$ is relatively small, the diffuse intensity is greatest near the Bragg peaks.

We have chosen a set of five realizations to illustrate this simple model. Four of these were obtained by Monte Carlo procedures and one obtained by growth-disorder model construction. Small representative portions of the diffraction masks derived from these realizations are shown in Fig. 2. For the purposes of

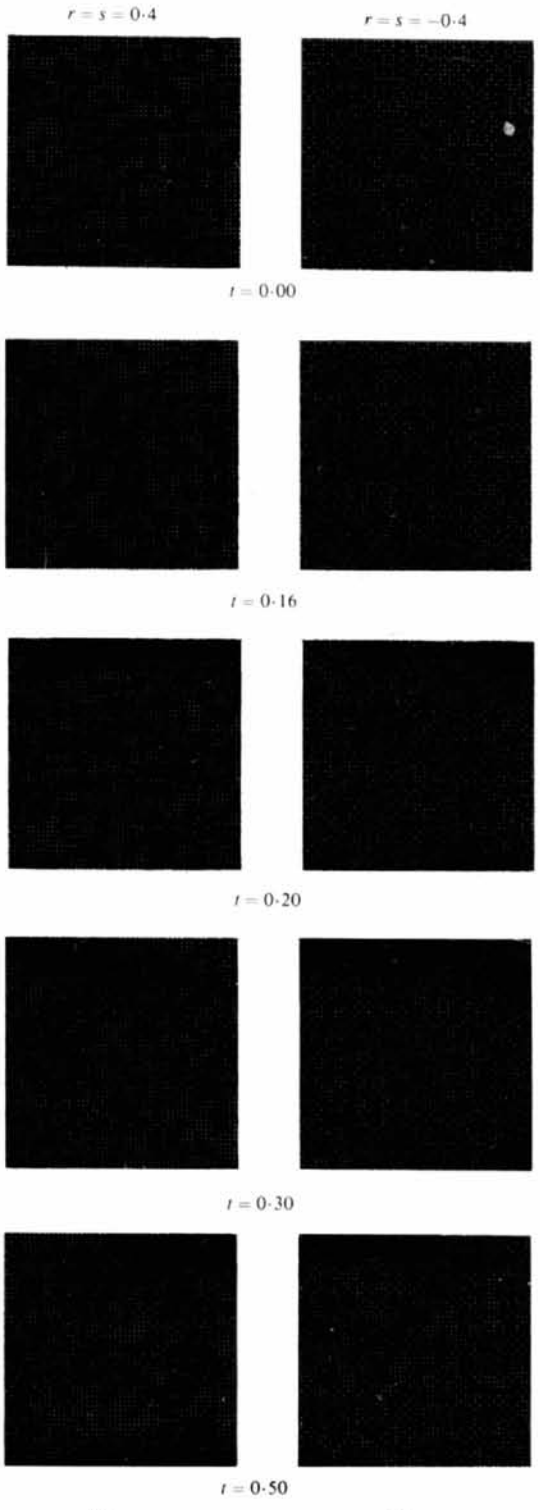

Fig. 2. Small portions of lattice realizations of the Gaussian model with (*a*) $r = s = 0{\cdot}4$ and (*b*) $r = s = -0{\cdot}4$, for different values of the diagonal correlation t. The realizations shown were obtained from the original variable density realizations by putting a 'dot' to represent densities greater than average and a 'blank' to represent those less than average. See text for details.

illustration we have converted the Gaussian variables to binary ones in the manner described by Welberry & Carroll (1982), since realizations in which the scattering points varied in density gave poor reproductions. In Fig. 2, therefore, the 'dots' represent atoms with above-average scattering power while 'blanks' represent atoms with below-average scattering power. The diffraction patterns shown in Fig. 3, however, were obtained from the Gaussian variable-density realizations themselves.

For the purpose of this illustration we chose the series $r = s = 0{\cdot}4$, and reference to (12) indicates a possible range of $-0{\cdot}2 < t < 1{\cdot}0$. Since the growth-disorder case lies closer to the lower end of this range we chose one example below it and three above it. The values of A, $B = C$, and D, together with some of the low-order correlation coefficients obtained *via* (15) by numerical integration, are given in Table 1. In Figs. 2 and 3 we also give examples for $r = s = -0{\cdot}4$. These could have been obtained by reversing the signs of B and C in the Monte Carlo procedure but were in fact obtained by reversing the signs of the random variables of the corresponding $r = s = 0{\cdot}4$ cases for lattice points such that $m + n$ is even. Similarly available without further Monte Carlo work would be the cases $r = 0{\cdot}4$, $s = -0{\cdot}4$ and $r = -0{\cdot}4$, $s = 0{\cdot}4$, by changing the signs of the random variables in alternate columns or rows.

For both positive and negative series, the diffraction patterns change dramatically over the range of t illustrated. In one extreme the diffuse 'peak' appears to be little more than the intersection of two diffuse bands of almost uniform intensity along their length. At $t = 0{\cdot}3$ the diffuse peaks are much more rounded and appear as distinct peaks with no sign of connecting diffuse bands. Between these values there is a gradual change including the growth-disorder case which, while exhibiting distinct 'peaks', nevertheless shows some of the diffuse banding along the axial directions. For $t = 0{\cdot}5$ the diagonal interaction dominates and the appearance of extra diffuse peaks corresponding to the repeat in the two sublattices ($m + n$ even and odd) suggests that a description in terms of these two sublattices is more appropriate in this case, with a weaker interaction connecting them.

The rounded appearance of the peaks in the $t = 0{\cdot}3$ cases leads us to consider the question of isotropy. Because of the fact that the distribution is based on a square lattice, no truly isotropic distribution can result, but various criteria for approximate isotropy can be formulated. We have used three different criteria. For the first two we choose t to make $\rho_{m,n}$ into a function of $m^2 + n^2$ such that there are alternative correlation coefficients. The first such value is $m^2 + n^2 = 25$. The corresponding criterion, $\rho_{4,3} = \rho_{5,0}$, is useful because one of these correlations is along the axis and the other approximately along the diagonal. In Table 1, we include the ratios of these two correlation coefficients.

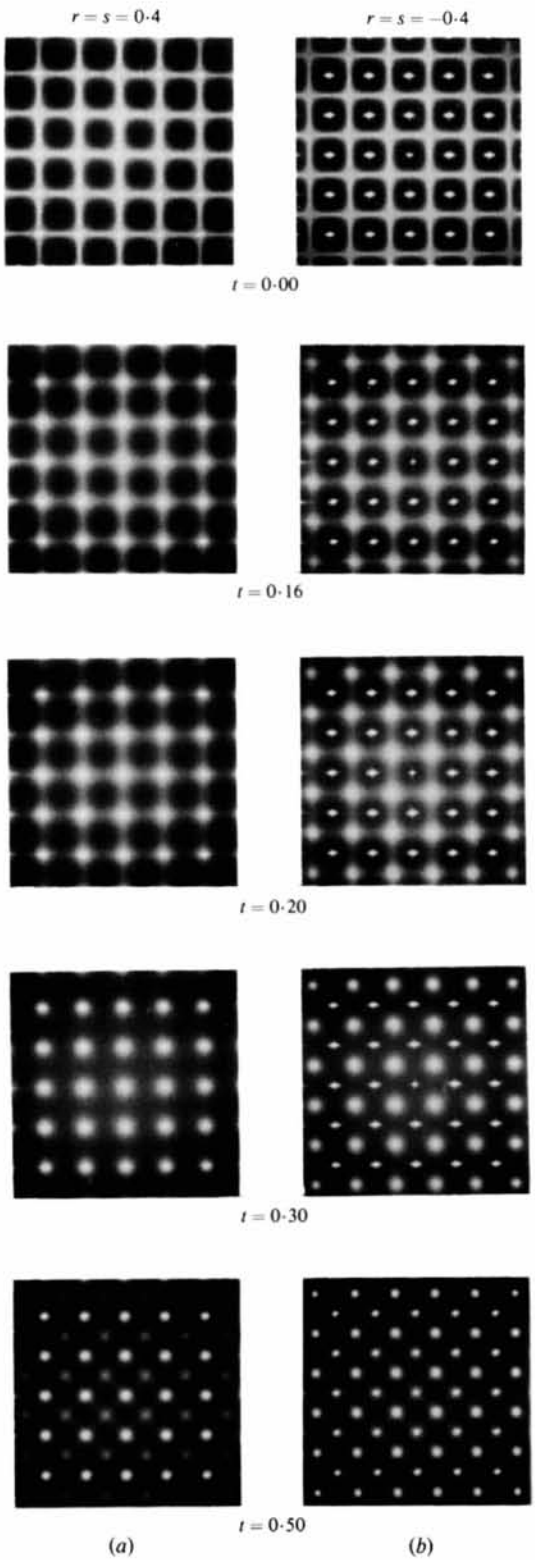

Fig. 3. Optical diffraction patterns obtained from the variable-density realizations of the Gaussian model with (*a*) $r = s = 0{\cdot}4$ and (*b*) $r = s = -0{\cdot}4$, for different values of the diagonal correlation t. See Table 1 for parameters.

Table 1. *Parameters used to generate the realizations shown in Fig. 2*

Also given are values of some low-order correlation coefficients $\rho_{m,n}$, and the ratios used to test isotropy, $\rho_{5,0}/\rho_{4,3}$ and B/D.

A	$B=C$	D	1 0	1 1	2 0	2 1	2 2	$\rho_{5,0}/\rho_{4,3}$	B/D
3·74872	−1·71795	0·86259	0·4000	0·0000	0·2336	−0·0408	−0·0363	−22·538	−1·9916
1·90703	−0·65760	0·22676	0·4000	0·1600	0·1600	0·0640	0·0256	6·250	−2·9000
1·73823	−0·52407	0·12535	0·4000	0·2000	0·1644	0·0969	0·0529	1·560	−4·1809
1·56888	−0·29349	−0·08275	0·4000	0·3000	0·2095	0·1830	0·1331	0·998	3·5467
1·93502	−0·07549	−0·40712	0·4000	0·5000	0·3884	0·3292	0·3292	0·993	0·1854

An alternative use of $\rho_{m,n}$ values as a criterion for isotropy is based on analytic evaluation of the behaviour of (15) as $m^2 + n^2 \to \infty$. This involves a saddle-point approximation; mathematical details are omitted.

A third criterion for isotropy is based on (19). We require the diffuse scattering to have circular peaks centred at each Bragg peak. Since (19) is a periodic function of Q_x and Q_y, the origin peak is typical. Near $Q_x = Q_y = 0$, the denominator becomes

$$(A + 2B + 2C + 4D) - (B + 2D)Q_x^2 - (C + 2D)Q_y^2 + \ldots \text{ etc.}$$

This power series shows that the small-angle scattering can be isotropic only if $B = C$. If we also make $B = 4D$ the denominator in (19) becomes

$$A + 5B - \tfrac{3}{2}B(Q_x^2 + Q_y^2) + \tfrac{1}{8}B(Q_x^2 + Q_y^2)^2 + \ldots, \quad (20)$$

and the diffuse scattering is as isotropic as possible within this model. The higher terms not shown explicitly in (20) cause a slight anisotropy. The ratios of B/D are included in Table 1.

In the present example of $r = s = 0{\cdot}4$, these three criteria for isotropy give values of t differing by less than 0·001. These three values of t are close to 0·30, for which the diffraction pattern is shown in Fig. 3, and for which the peaks are clearly approximately isotropic. Calculations of the correlation coefficients show that the deviations from isotropy are smaller for $t = 0{\cdot}5$ than for $t = 0{\cdot}2$. This is also shown by the diffraction patterns in Fig. 3.

5. Random displacements

In our second application of the Gaussian model, one atom is associated with each site of a square lattice, and the displacements of atoms from their lattice sites are random variables. We assume that the horizontal components of the atomic displacements are statistically independent of the vertical components, and we use two separate realizations of our multivariate Gaussian model for these components. The resulting intensity of diffuse scattering is discussed in this section. The growth-disorder special case of this model was discussed by Welberry, Miller & Carroll (1980) and Welberry & Carroll (1982).

We again suppose $\mathbf{l}$ is a vector from the origin to a lattice site; it has integer components m and n. The corresponding atomic position is $\mathbf{l} + \mathbf{d}$, and the atomic form factor is unity. Because of the translational invariance of the statistical properties, we define the intensity function as

$$I(\mathbf{Q}) = \sum_l \exp[i\mathbf{Q}.\mathbf{l}]\,\langle\exp[i\mathbf{Q}.(\mathbf{d}_l - \mathbf{d}_0)]\rangle.$$

Since $\mathbf{Q}.(\mathbf{d}_l - \mathbf{d}_0)$ is a Gaussian random variable with zero mean, this becomes

$$I(\mathbf{Q}) = \sum_l \exp\{i\mathbf{Q}.\mathbf{l} - \tfrac{1}{2}\langle[\mathbf{Q}.(\mathbf{d}_l - \mathbf{d}_0)]^2\rangle\}$$
$$= \exp(-2W)\sum_l \exp[i\mathbf{Q}.\mathbf{l} + \langle(\mathbf{Q}.\mathbf{d}_l)(\mathbf{Q}.\mathbf{d}_0)\rangle].$$

The Debye–Waller factor, $\exp(-2W) = \exp[-\langle(\mathbf{Q}.\mathbf{d}_0)^2\rangle]$, depends on the mean square of the atomic displacements. The variances in our Gaussian model are $\sigma^2 = \langle X_{00}^2\rangle = \langle Y_{00}^2\rangle$, and this gives $\exp(-2W) = \exp[-(Q_x^2 + Q_y^2)\sigma^2]$. The Bragg component of the intensity is

$$I(\mathbf{Q})_{\text{Bragg}} = \exp(-2W)\sum_l \exp(i\mathbf{Q}.\mathbf{l}).$$

The diffuse component of the intensity is

$$I(\mathbf{Q})_{\text{diff}} = \exp(-2W)\sum_l \exp(i\mathbf{Q}.\mathbf{l}) \times \{\exp[\langle(\mathbf{Q}.\mathbf{d}_l)(\mathbf{Q}.\mathbf{d}_0)\rangle] - 1\}, \quad (21)$$

and

$$\langle(\mathbf{Q}.\mathbf{d})\,(\mathbf{Q}.\mathbf{d}_0)\rangle = Q_x^2\langle X_{mn}X_{00}\rangle + Q_y^2\langle Y_{mn}\,Y_{00}\rangle.$$

We assume that the primary correlation coefficients r and s are associated with longitudinal and transverse correlations of atomic displacements, respectively. This means that the horizontal correlations of the Y variables are the same as the vertical correlations of the X variables and that $\langle Y_{mn}Y_{00}\rangle = \langle X_{nm}X_{00}\rangle$. The covariances $\langle X_{mn}X_{00}\rangle$ are given by (6). Use of the power series for the last exponential function in (21) gives

$$I(\mathbf{Q})_{\text{diff}} = \exp(-2W)\sum_{P=1}\frac{1}{P!}\sum_{m,n}\exp(imQ_x + inQ_y) \times \left[\frac{1}{N}\sum_{\lambda,\mu}\frac{Q_x^2\exp(im\lambda + in\mu) + Q_y^2\exp(in\lambda + im\mu)}{A + 2B\cos\lambda + 2C\cos\mu + 4D\cos\lambda\cos\mu}\right]^P. \quad (22)$$

Table 2. *Parameters used to generate the realizations shown in Fig.* 4

Also given are values of some low-order correlation coefficients $\rho_{m,n}$, and the ratios used to test isotropy, $\rho_{5,0}/\rho_{4,3}$ and B/D.

A	$B=C$	D	1 0	1 1	2 0	2 1	2 2	$\rho_{5,0}/\rho_{4,3}$	B/D
90·75069	−45·12465	22·43767	0·9000	0·8100	0·8100	0·7290	0·6561	1·2346	−2·0111
13·86128	−5·39596	1·93064	0·9000	0·8500	0·8356	0·8100	0·7848	1·0077	−2·7949
9·63340	−1·95010	−0·45825	0·9000	0·8800	0·8612	0·8548	0·8418	1·0000	4·2556
10·00000	−0·94031	−1·55970	0·9000	0·9000	0·8805	0·8757	0·8683	0·9996	0·6029
19·83720	−0·04070	−4·91860	0·9000	0·9500	0·9367	0·8990	0·9283	1·0000	0·0083

This infinite series is a generalization of one that appeared in Welberry, Miller & Carroll (1980). To simplify each term, we evaluate the sums over m and n. As in the previous section, we may assume that Q_x and Q_y are equal to allowed values of λ and μ, respectively. Then two more sums can be done easily, which leaves $2P-2$ sums in the P'th term. In the limit of an infinite lattice, the result is

$$
\begin{aligned}
I(\mathbf{Q})_{\text{diff}} = {} & Q_x^2 \exp(-2W)[A + 2B\cos(Q_x) \\
& + 2C\cos(Q_y) + 4D\cos(Q_x)\cos(Q_y)]^{-1} \\
& + Q_y^2 \exp(-2W)[A + 2B\cos(Q_y) \\
& + 2C\cos(Q_x) + 4D\cos(Q_y)\cos(Q_x)]^{-1} \\
& + \int_{-\pi}^{\pi}\int \frac{d\lambda\, d\mu}{(2\pi)^2}[\exp(-2W)/2!](A + 2B\cos\lambda \\
& + 2C\cos\mu + 4D\cos\lambda\cos\mu)^{-1} \\
& \times \{Q_x^4[A + 2B\cos(Q_x+\lambda) + 2C\cos(Q_y+\mu) \\
& + 4D\cos(Q_x+\lambda)\cos(Q_y+\mu)]^{-1} \\
& + Q_y^4[A + 2B\cos(Q_y+\lambda) + 2C\cos(Q_x+\mu) \\
& + 4D\cos(Q_x+\mu)\cos(Q_y+\lambda)]^{-1} \\
& + Q_x^2 Q_y^2[A + 2B\cos(Q_x+\mu) + 2C\cos(Q_y+\lambda) \\
& + 4D\cos(Q_x+\mu)\cos(Q_y+\lambda)]^{-1} \\
& + Q_x^2 Q_y^2[A + 2B\cos(Q_y+\mu) + 2C\cos(Q_x+\lambda) \\
& + 4D\cos(Q_x+\lambda)\cos(Q_y+\mu)]^{-1}\} \\
& + \int\int_{-\pi}^{\pi}\int\int \frac{d\lambda\, d\mu\, d\lambda'\, d\mu'}{(2\pi)^4} \\
& \times (\text{terms in } Q_x^6,\ Q_x^4 Q_y^2,\ Q_x^2 Q_y^4, \text{ and } Q_y^6) + \ldots . \quad (23)
\end{aligned}
$$

As examples to illustrate this displacement model we choose examples which are 'paracrystal-like'. This occurs when the standard deviation, σ, is sufficiently large that no Bragg peaks are discernible because of the very small Debye–Waller factor. At the same time the nearest-neighbour correlations are high so that the standard deviation of the distance between neighbours is still moderately small. In such cases the diffuse diffraction pattern reflects the local ordering with pronounced peaks. For further details see Welberry, Miller & Carroll (1980).

For the present purposes we chose the series $r = s = 0{\cdot}9$ for which t may vary from 0·80 to 1·0. The growth-disorder case has $t = 0{\cdot}81$ and in addition to this we show four examples with $t > 0{\cdot}81$. Difficulties were encountered with the Monte Carlo procedure for examples approaching the lower limiting value of 0·8 and so these were not pursued. In Table 2 we list the values of A, $B = C$, D; some low-order correlation values; and the ratios $\rho_{4,3}/\rho_{5,0}$ and B/D for the chosen set of examples. Small representative portions of lattice realizations are shown in Fig. 4 and their corresponding diffraction patterns in Fig. 5. In Table 2 the values of A, B, D refer to $\sigma^2 = 1$ and to obtain actual realizations the random numbers were scaled to the appropriate values as a fraction of the cell repeat. For example, in Fig. 4 we show realizations with two different values of σ^2 for each example, which were obtained in this way from the same unit-variance distributions.

To understand these diffraction patterns we consider the intensity (23), remembering that for these high values of σ^2 we require to consider many terms of the summation over P of (22). In (23) we see that the coefficients of Q_x^2 and Q_y^2 in the first terms have the simple form (19). Since we have large values of r, s, t this first term will produce a contribution to the intensity very like one of the patterns of Fig. 3 but with much sharper peaks. The second group of terms in (23), involving Q_x^4, Q_y^4, and $Q_x^2 Q_y^2$, are convolutions of two functions of the form (19). Thus, each of these terms represents a function in which the sharp peaks of the first term have been smeared somewhat, but nevertheless having a similar overall periodic distribution. Further terms not given explicitly, involving integrals of a higher multiplicity, consist of even more greatly smeared versions of the basic intensity function (19).

Finally we consider the variation with $\mathbf{Q}$. At sufficiently small $\mathbf{Q}$ the first term dominates, but in our present example this will only occur at values of $\mathbf{Q}$ which are very small fractions of 2π. At higher values of $\mathbf{Q}$ the contribution of the Pth term is weighted by factors depending on $\mathbf{Q}^P$ and $1/P!$. For any given $\mathbf{Q}$ the contribution of the P'th term eventually falls rapidly with increasing P, but the higher the value of $\mathbf{Q}$, the

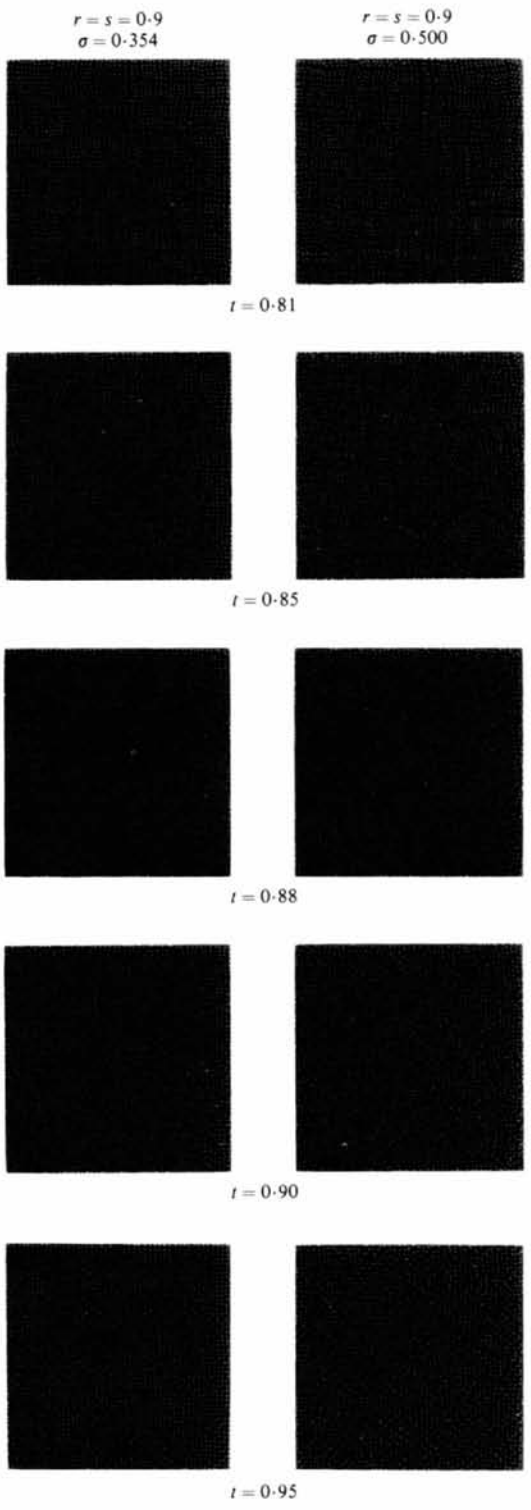

Fig. 4. Small representative portions of realizations in which the displacements of points from an underlying regular lattice are random variables distributed according to a 2D Gaussian model. In the examples shown $r = s = 0{\cdot}9$ and t is varied. σ is the standard deviation of the displacements expressed as a fraction of the cell edge. See Table 2 for parameters.

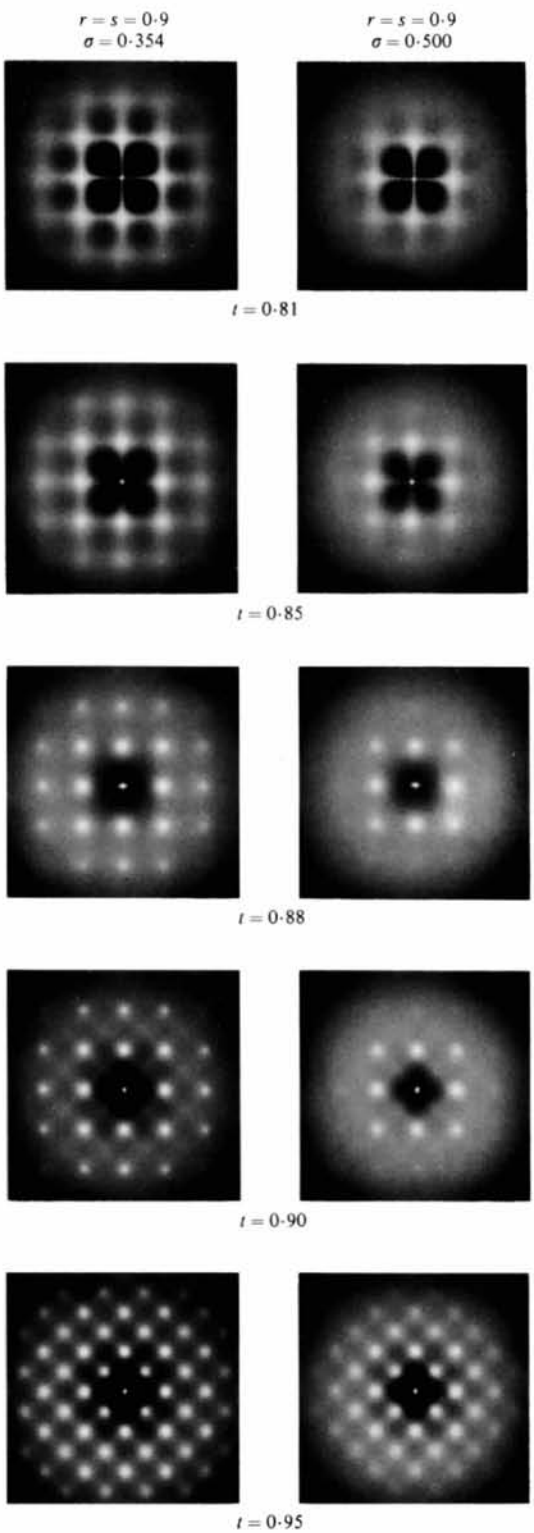

Fig. 5. Optical diffraction patterns corresponding to the realizations of the displacement model shown in Fig. 4. For these examples $r = s = 0{\cdot}9$ and t is varied. σ is the standard deviation of the displacements expressed as a fraction of the cell edge. See Table 2 for parameters.

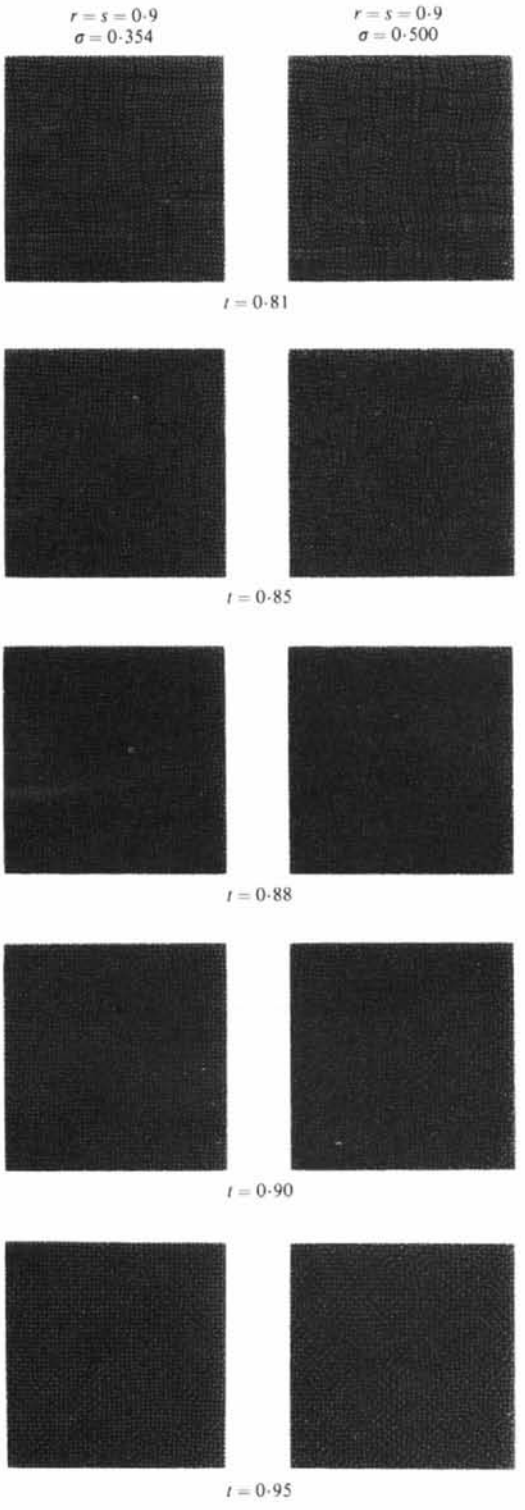

Fig. 4. Small representative portions of realizations in which the displacements of points from an underlying regular lattice are random variables distributed according to a 2D Gaussian model. In the examples shown $r = s = 0{\cdot}9$ and t is varied. σ is the standard deviation of the displacements expressed as a fraction of the cell edge. See Table 2 for parameters.

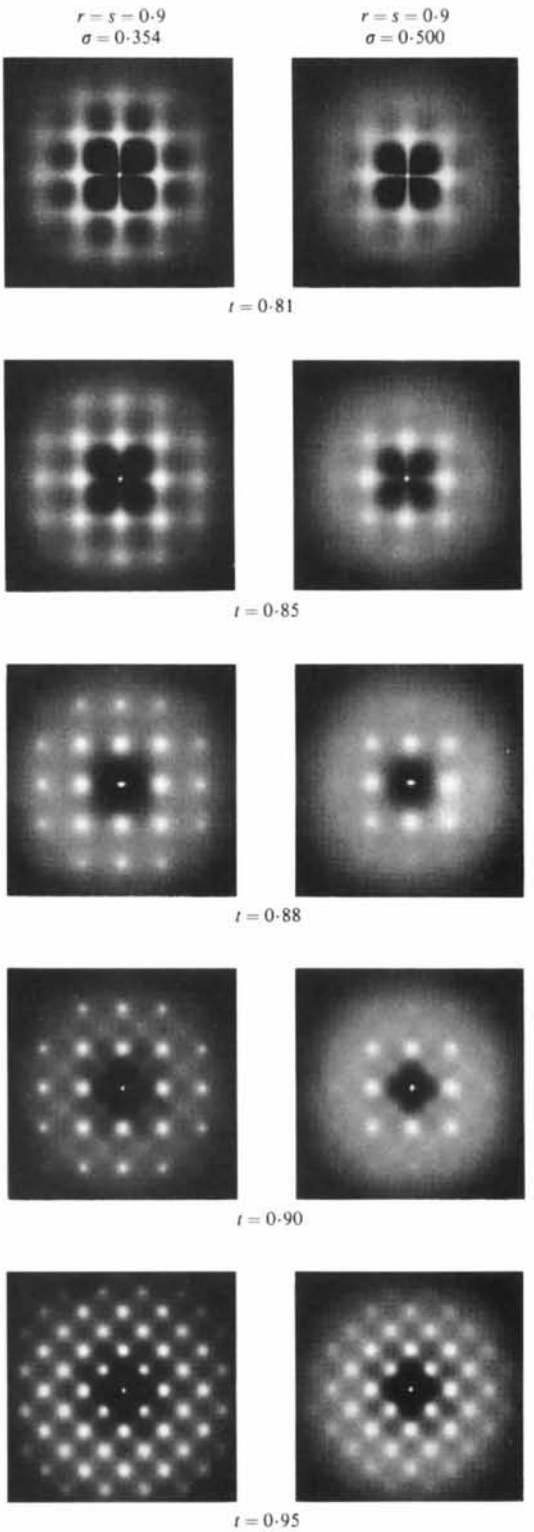

Fig. 5. Optical diffraction patterns corresponding to the realizations of the displacement model shown in Fig. 4. For these examples $r = s = 0{\cdot}9$ and t is varied. σ is the standard deviation of the displacements expressed as a fraction of the cell edge. See Table 2 for parameters.

more terms are required. Thus at low diffraction angles the more highly peaked distributions dominate the pattern while at progressively higher angles the more highly smeared distributions take over. This result is familiar in the context of paracrystals.

Many of the t-dependent features of the simple example illustrated in Fig. 3 are also apparent in the diffraction patterns of Fig. 5. Notable is the greater isotropy of the diffuse peak shapes at the higher values of t, and the accompanying sharper peak profiles. For this series the most isotropic case according to the criteria listed in § 4 occurs close to $t = 0{\cdot}880$ and, while the diffuse peaks for this case and the $t = 0{\cdot}9$ case appear little different, the greater isotropy is evident in the shape of the dark region occurring at low diffraction angles. In the growth-disorder case which approximates the 'ideal paracrystal' the characteristic 'maltese-cross'-shaped appearance of the low-angle scattering is very evident. This feature was prominent in the discussion of the paracrystal model by Brämer & Ruland (1976).

6. Monte Carlo simulations

The standard Monte Carlo technique devised by Metropolis, Rosenbluth, Rosenbluth, Teller & Teller (1953) generates a Maxwell–Boltzmann distribution. To apply it, we regard the exponential function in (5) as the Boltzmann factor. The computation proceeds as follows. We first set up an initial array of Gaussian-distributed random variables of unit variance and zero correlations (or we use a realization from a previous run). One point in the array is chosen at random and the random variable at that site adjusted by a small random shift. The energy of this new configuration is then compared to the old. If the new configuration is of a lower energy this configuration is certainly accepted, but if it is higher in energy it is only accepted with a probability of $\exp(-\Delta E/kT)$, where ΔE is the energy difference. A new point in the array is then chosen and the procedure is repeated. At each iteration the computation of $\Delta E/kT$ from (5) requires use of the eight random variables surrounding the point considered. Many iterations are required to achieve equilibrium and it is convenient to refer to a 'cycle of refinement', by which we mean the number of iterations required to access, on average, each point in the array once.

Since distant variables separated by, say, n cell vectors cannot possibly influence each other in less than n cycles of refinement, the amount of computation necessary depends on the magnitude of the correlations required. Thus, for the examples of Figs. 2 and 3 where the short-range order extends only a few lattice spacings about 20–25 cycles were performed. On the other hand, for the examples of Figs. 4 and 5 which involve much higher correlations a much larger number of cycles (>100) was employed. Progress of the refinement was monitored by calculating the lattice averages (3) after each cycle. Also monitored was the acceptance/rejection ratio for the new configuration, and on subsequent cycles the magnitude of the random shift was adjusted accordingly to obtain an acceptance ratio close to 0·5. During refinement, when the configuration was still some way from equilibrium, we found there was a tendency for the variance of the random variables to drift away from unity. After each cycle this was corrected by renormalization of the variables, and as equilibrium was approached the tendency disappeared.

The experiments were performed on an array of 512×512 points, to be consistent with earlier growth-disorder realizations. Periodic boundary conditions were imposed. Since it was not feasible to store such a large array in computer memory, a procedure was adopted whereby a subarray of 70×70 points was selected at random from the main array which was maintained on a disk. After a cycle of refinement on this subarray, it was returned to the disk and a further subarray selected. In this way it was possible to obtain realizations using only our PDP 11/45 minicomputer.

In order to check the validity of the computer program and the criteria for equilibrium, we performed Monte Carlo runs using the parameters for the growth-disorder model case $r = s = 0{\cdot}9$, $t = 0{\cdot}81$. The realizations obtained, while evidently still a little way from achieving the true equilibrium of the growth-disorder model construction, nevertheless gave diffraction patterns barely distinguishable from those of the latter. We thus have reasonable confidence that the diffraction patterns we have obtained truly reflect the properties of the Gaussian model.

The optical diffraction masks of lattice realizations were produced from the final array of Gaussian variables using an Optronics P-1700 Photomation system (see Harburn, Miller & Welberry, 1974). In all cases the basic grid used was a 200×200 μm square. For the variable-density realizations used to obtain the diffraction patterns of Fig. 3, lattice points were plotted with a mean optical density of 127 on a scale where 255 represents the maximal optical density of about $2{\cdot}4D$. The standard deviation used was 40 units so that variables within about 3σ of the mean were satisfactorily represented. The small number of variables outside this range were given a zero or a maximum density. For the displacement realizations of Fig. 4, each point was positioned to the nearest 12·5 μm, the basic raster size of our Photomation system.

7. Discussion

The properties of the multivariate Gaussian model which we have described in this paper have enabled us

to place in context the crystal growth-disorder models which have been of particular use in generating realizations of disordered lattice distributions for optical diffraction analogue experiments of disorder problems in real crystals. Our experiences in the present work have reaffirmed that, for the size of sample that is required for this purpose, the generation of realizations by growth-disorder algorithms is at least two orders of magnitude quicker than use of the Monte Carlo procedures which are necessary for the more general cases. Nevertheless we have found that the extra degree of freedom afforded by the general model allows considerable further diversity in the diffraction patterns.

At this stage it is not clear which examples of the general model might correspond most closely to real crystal situations. It would appear that the more extreme of the permissible values of the diagonal correlation, t, might correspond to situations where the model could well be reformulated more simply on a different lattice, but despite this there still remains, for intermediate values of t, a range of models, and it is unclear which is the most suitable for emulating real disorder problems. Our experience with orientational disorder in molecular crystals suggests that when the primary correlations in two different directions are approximately equal in magnitude, the peaks in the disorder diffuse scattering have a more rounded appearance than those given by a growth-disorder model. Such was the case, for example, in the $0kl$ section of orthorhombic 9-bromo-10-methyl-anthracene (Welberry, Jones & Epstein, 1982). For this reason we believe that models closer to that for which the isotropy condition is satisfied might be more appropriate than the growth-disorder case. For situations where the primary correlations, r and s, are not equal, a simple extension of the isotropy ideas of § 4 could be to suppose that the correlations are a function of $\alpha m^2 + \beta n^2$ where α and β are positive constants.

From the point of view of interpreting real X-ray diffraction patterns an important consideration is the effect of the choice of model on the estimation of the primary correlations. A number of workers, *e.g.* Flack (1970), Glazer (1970), have used a measurement of peak width at half-height to estimate short-range-order parameters; a method described by Wilson (1962). This method relies on the characteristic peak profile shape which results from geometrically decaying correlations. Such geometric correlations are valid for simple one-dimensional nearest-neighbour problems or for our growth-disorder model, but are not generally to be expected for two- and three-dimensional problems. In particular we note from the present work that correlations decay more slowly for the isotropic case than for the growth-disorder model with the same r and s. This results in a sharper peak profile, and its analysis assuming the standard peak profile would give erroneous results for the primary correlations. A second point that is relevant here is that the 'peak profile' should strictly refer to the projection of the diffuse scattering distribution onto a line in reciprocal space. Estimation of peak widths by taking a section through the diffuse peak, as for example done by Singh & Glazer (1981), will again lead to erroneous estimation of nearest-neighbour correlations unless the correlation field is geometric, since the measured reciprocal *section* corresponds to a *projection* of the correlation field onto a real-space axis.

In § 5 we have used the general Gaussian model to explore the generalization of the paracrystal-like lattices described in Welberry, Miller & Carroll (1980). Here too the question of which of the range of possible models is most appropriate must be considered by those working in the field. Some of the draw-backs of the 'ideal paracrystal', which is closely related to the growth-disorder-model special case of the present model, may be removed by moving to more isotropic examples of the model. In particular we note that the pronounced streaking in the axial directions at low angles is removed in examples away from the growth-disorder case. On the other hand, adoption of a more isotropic model would certainly alter the details of the interpretation of diffuse peak shapes to obtain neighbour statistics.

In conclusion we suggest that the present work indicates that while growth-disorder models in their present form remain useful in simulating disorder effects because of their rapid and simple use, sufficiently large differences in the form of the correlation field may exist in real crystals that their use may not always be appropriate for anything other than qualitative work. We would expect the appropriateness to be greatest, either when the problem involves basically one-dimensional disorder with only minor perturbations in other dimensions, or when the correlations involved are relatively small. In a previous paper (Welberry & Carroll, 1982) we have described ways in which growth-disorder models may be combined to produce a greater diversity of lattice realizations. While that work did not reveal ways in which the correlation field could be given the sort of isotropic properties found possible here, we are at present working on ways by which this may be achieved.

We are grateful to K. Owen for technical assistance.

APPENDIX

The computation of σ^2, r, s, t as functions of A, B, C, D and *vice versa* is based on equations (7)–(10). In this Appendix, we outline how these four integrals are evaluated, and how the resulting equations are solved for A, B, C, D.

The integrals (15) are complete elliptic integrals and can be reduced to normal form by standard substitutions; see a treatise such as Byrd & Friedman (1971). We may assume $AD - BC \neq 0$, for the growth-disorder case treated in § 3. We shall assume $D \neq 0$, and use

$$A + 2Br + 2Cs + 4Dt = 1/\sigma^2 \qquad (A1)$$

to evaluate t. Thus we reduce only (7), (8) and (9) to known functions. The first of these integrals is

$$\sigma^2 = (A + 2B \mp 2C \mp 4D)^{-1/2} \times (A - 2B \pm 2C \mp 4D)^{-1/2}(2K/\pi). \qquad (A2)$$

The upper sign applies if $t > rs$ and the lower sign if $t < rs$. K is the complete elliptic integral of the first kind, which can be written as

$$K = \tfrac{1}{2}\int_0^\infty [u(u+1)(u+k'^2)]^{-1/2}\,du. \qquad (A3)$$

The complementary modulus is

$$k' = \left[\frac{(A + 2B + 2C + 4D)(A - 2B - 2C + 4D)}{(A + 2B - 2C - 4D)(A - 2B + 2C - 4D)}\right]^{\pm 1/2}$$

We now treat (8), which involves the complete elliptic integral of the third kind. Equations (7) and (8) give

$$r + 1 = (R/K)\int_0^\infty (u+R)^{-1}[u(u+1)(u+k'^2)]^{-1/2}\,du, \qquad (A4)$$

where $R = (A - 2B \mp 2C \pm 4D)/(A + 2B \mp 2C \mp 4D)$. Interchange of B and C gives

$$s + 1 = (S/K)\int_0^\infty (u+S)^{-1}[u(u+1)(u+k'^2)]^{-1/2}\,du, \qquad (A5)$$

where $S = (A \mp 2B - 2C \pm 4D)/(A \mp 2B + 2C \mp 4D)$. Equations (A1)–(A5) provide the means for computing σ^2, r, s, t as functions of A, B, C, D. The integrals in (A4) and (A5) are in one of the Zill–Carlson (1970) normal forms for elliptic integrals of the third kind. The integrals in (A3), (A4) and (A5) can conveniently be evaluated by the Carlson (1979) algorithms, which are available as NAG Fortran routines.

In the converse problem, it is convenient to compute k', R, S as functions of r, s, t before computing A, B, C, D. For any fixed values of r, s and k', (A4) and (A5) can be solved for R and S; we have used a rapidly convergent form of Regula Falsi (Dowell & Jarratt, 1972) to do this. Then an equation derived from (A1) can be used to compute t. The target value of t is subtracted from the computed value, and this whole procedure is repeated for a different value of k'. Another use of Regula Falsi leads to the correct value of k'. Finally, we compute A, B, C, D, using

$$A = \frac{(k'^2 + R + S + RS)K}{2\pi\sigma^2(RS)^{1/2}},$$

$$B = \frac{(k'^2 - R + S - RS)K}{4\pi\sigma^2(RS)^{1/2}},$$

$$C = \frac{(k'^2 + R - S - RS)K}{4\pi\sigma^2(RS)^{1/2}},$$

$$D = \frac{(k'^2 - R - S + RS)K}{8\pi\sigma^2(RS)^{1/2}},$$

if $t > rs$, and

$$A = \frac{[k'^2(1 + R + S) + RS]K}{2\pi\sigma^2 k'(RS)^{1/2}},$$

$$B = \frac{[k'^2(1 - R + S) - RS]K}{4\pi\sigma^2 k'(RS)^{1/2}},$$

$$C = \frac{[k'^2(1 + R - S) - RS]K}{4\pi\sigma^2 k'(RS)^{1/2}},$$

$$D = \frac{[k'^2(1 - R - S) + RS]K}{8\pi\sigma^2 k'(RS)^{1/2}},$$

if $t < rs$.

References

BRÄMER, R. & RULAND, W. (1976). *Makromol. Chem.* **177**, 3601–3617.

BYRD, P. F. & FRIEDMAN, M. D. (1971). *Handbook of Elliptic Integrals for Engineers and Scientists*, 2nd ed., revised. Berlin: Springer.

CARLSON, B. C. (1979). *Numer. Math.* **33**, 1–16.

CHENG, H. & WU, T. T. (1967). *Phys. Rev.* **164**, 719–735.

DOWELL, M. & JARRATT, P. (1972). *BIT, Nord. Tidskr. Infbehandl.* **12**, 503–508.

FLACK, H. D. (1970). *Philos. Trans. R. Soc. London Ser. A*, **266**, 559–591.

GLAZER, A. M. (1970). *Philos. Trans. R. Soc. London Ser. A*, **266**, 593–639.

HARBURN, G., MILLER, J. S. & WELBERRY, T. R. (1974). *J. Appl. Cryst.* **7**, 36–38.

HOSEMANN, R. & BAGCHI, S. N. (1962). *Direct Analysis of Diffraction by Matter*. Amsterdam: North-Holland.

HOSEMANN, R., VOGEL, W., WEICK, D. & BALTÁ-CALLEJA, F. J. (1981). *Acta Cryst.* A**37**, 85–91.

METROPOLIS, N., ROSENBLUTH, A. W., ROSENBLUTH, M. N., TELLER, A. H. & TELLER, E. (1953). *J. Chem. Phys.* **21**, 1087–1092.

MONTROLL, E. W., POTTS, R. B. & WARD, J. C. (1963). *J. Math. Phys.* **4**, 308–322.

MORAN, P. A. P. (1973*a*). *J. Appl. Probab.* **10**, 54–62.

MORAN, P. A. P. (1973*b*). *J. Appl. Probab.* **10**, 605–612.

SINGH, S. & GLAZER, A. M. (1981). *Acta Cryst.* A**37**, 804–808.

WELBERRY, T. R. (1977). *Proc. R. Soc. London Ser. A*, **353**, 363–376.
WELBERRY, T. R. (1982). *Acta Cryst.* B**38**, 1921–1927.
WELBERRY, T. R. & CARROLL, C. E. (1982). *Acta Cryst.* A**38**, 761–772.
WELBERRY, T. R., JONES, R. D. G. & EPSTEIN, J. (1982). *Acta Cryst.* B**38**, 1518–1525.
WELBERRY, T. R., MILLER, G. H. & CARROLL, C. E. (1980). *Acta Cryst.* A**36**, 921–929.
WELBERRY, T. R., MILLER, G. H. & PICKARD, D. K. (1979). *Proc. R. Soc. London Ser. A*, **367**, 175–192.
WILSON, A. J. C. (1962). *X-ray Optics*, 2nd ed. London: Methuen.
ZILL, D. G. & CARLSON, B. C. (1970). *Math. Comput.* **24**, 199–214.

Acta Cryst. (1983). A**39**, 245–251

Tensor Properties and Rotational Symmetry of Crystals. III. Use of Symmetrized Components in Group $3(3_z)$*†

BY F. G. FUMI AND C. RIPAMONTI

Istituto di Scienze Fisiche, Universitá di Genova, Italy and GNSM-CNR, Unitá di Genova, Italy

(*Received* 18 *February* 1981; *accepted* 20 *October* 1982)

Abstract

'Symmetrized' components are introduced in place of the standard ones to improve the method presented in paper I [Fumi & Ripamonti (1980). *Acta Cryst.* A**36**, 535–551]. These components, which are simply related to the standard ones, allow a further reduction of the computational task and also a further simplification of the results and of their use. This is illustrated by application to general two-dimensional tensors of ranks 6 and 8 and by particularization of the results to the cases of the third- and fourth-order elastic tensors.

Introduction

In this paper we introduce symmetrizations in tensor space with respect to the standard reference directions x and y, perpendicular to the principal symmetry axis along the z direction, to improve the method presented in paper I (Fumi & Ripamonti, 1980*a*). From I such symmetrizations allow a further splitting of a tensor invariant in group $3(3_z)$ into independent subtensors: this splitting is additional to the standard ones (see I, § 3*b*) already exploited by the method and concerns only subtensors of even rank in x and y.

* Supported in part by a NATO Research Grant. Part of the 'Tesi di Perfezionamento in Fisica' to be submitted by C. Ripamonti to the University of Genoa.

† We refer the reader to Paper I (Fumi & Ripamonti, 1980*a*) for the details of the method and for the pertinent notations.

0567-7394/83/020245-07$01.50

1. Symmetrized components

(*a*) *Definition and splitting*

For subtensors of even rank in x and y, we introduce symmetrizations with respect to x,y exchange by defining 'symmetrized components' as follows:

$$c^+ = c + \tilde{c} \tag{1}$$

and

$$c^- = c - \tilde{c} \tag{2}$$

for every pair of standard components c and $\tilde{c}$ related by an x,y exchange. From the identity – except for sign – of the coefficients of c and $\tilde{c}$ in the tensor invariants for group $3(3_z)$ in Hermann's base [see I, § 3*c* and Appendix (iii)], it follows that the c^+'s and c^-'s have non-zero coefficients only in disjoint sets of invariants as follows:

c^+'s of even rank in x and in y (even parity in x and in y),	Re-type invariants of the $n_+ = n_-$ mod 4 subtype	(3)
c^-'s of even rank in x and in y,	Re-type invariants of the $n_+ \neq n_-$ mod 4 subtype	(4)
c^+'s of odd rank in x and in y (odd parity in x and in y),	Im-type invariants of the $n_+ \neq n_-$ mod 4 subtype	(5)
c^-'s of odd rank in x and in y,	Im-type invariants of the $n_+ = n_-$ mod 4 subtype.	(6)